EXPERIMENTAL AND CFD ANALYSIS OF WIRE COIL TURBULATORS IN BIOMASS BOILERS

by

Djordje A. NOVČIĆ[a], Miloš V. NIKOLIĆ[a], Dušan M. TODOROVIĆ[b], Rade M. KARAMARKOVIĆ[a*], and Marko O. OBRADOVIĆ[b]

[a] Faculty of Mechanical and Civil Engineering in Kraljevo, University of Kragujevac, Kragujevac, Serbia
[b] Faculty of Mechanical Engineering, University of Belgrade, Belgrade, Serbia

Original scientific paper
https://doi.org/10.2298/TSCI2301071N

To achieve as complete fuel burnout with as little excess air as possible, small wood log boilers (< 50 kW) use stage combustion. The first stage is often a process similar to downdraft gasification that consequently produces a flue gas laden with particulates. To prevent the build-up of solids and promote heat transfer in pipes of the convective part of these boilers, wire coils are used. The paper presents their in-situ examination together with CFD analysis. The analysis is carried out in a 460 mm long pipe, with a diameter of 82.5 mm, equipped with different wire coils for flue gas temperatures in the range between 300 °C and 150 °C. The analyzed coils are with and without a conical spring at their free end. The addition of this conical top is economical and should influence the rotation of the core flow. Proper pipe surface cleaning limited the analyzed wire coil designs to the dimensionless pitch, p/d, in the range between 0.36-0.61, dimensionless wire diameter e/d = 0.04-0.1, and pitch to wire diameter ratios p/e = 3.75-14.3, and three different angles (60º, 90º, and 120º) of the conical top. The goals are to find the optimal flue gas velocity for the given operating conditions, pipe, and wire coil dimensions, and to investigate the addition of the conical top on heat transfer enhancement. Several evaluation criteria are used to achieve the goals.

Key words: *wire coils, heat transfer enhancement, turbulators, CFD model, biomass boiler*

Introduction

Although traditional biomass, like fuelwood and charcoal, accounts for only 20% of wood used in temperate regions [1], its use is significant and, together with stringent regulations regarding energy efficiency and flue gas emissions, prompts the continual improvement of small residential boilers. These boilers frequently implement refractory inserts, turbulators, and systems that utilize the higher heating value of the fuel to achieve as complete combustion as possible and improve their efficiency. Refractories are used to preheat the fuel and combustion air, sustain the gas phase at a high temperature, improve heat transfer, enable the usage of relatively moist biomass, and remove particulates from the flue gas. The higher heating value of the fuel is utilized by the use of flue gas condensers [2] or by the implementation of active condensation [3].

* Corresponding author, e-mail: karamarkovic.r@mfkv.kg.ac.rs

To enhance heat transfer in pipe exchangers, active, passive, and compound methods are used [4]. In small biomass boilers, the majority of heat transfer enhancement devices belong to the passive method as they do not need external power input. There are numerous designs: twisted, see *e.g.*, [4, 5], and sinusoidal [6] tapes, wire coils, ribs [4, 7], swirl generators [8], conical [9, 10], and circular [11] rings, *etc*. The number of applicable turbulator types decreases if the prevention of surface fouling and heat transfer enhancement are simultaneously required. Wire coils meet both criteria and are one of the most frequently used, economical, and simple designs. Helical pitch, see p in fig. 1(a), and the diameters of wire, e, and pipe, d, define their geometry. In the segment of small biomass boilers where convective heat transfer dominates, flue gas velocities are typically in the transition flow regime. Regarding that, the important features of wire coils are:

– their best performance is within the transition region, where heat transfer augmentation depends strongly on Prandtl number [12],
– the transition to turbulent flow takes place at low Reynolds numbers (Re < 700) and in a gradual way [13], therefore,
– wire coils have a predictable behavior within the transition region since they show continuous curves of friction factor and Nusselt number [12].

The works of Garcia *et al.* [12], Hong *et al.* [14], and Gholamalizadeh *et al.* [15] review experimental and numerical research work by other authors and present modifications in the design of wire coils over time. These works and design changes can be divided into:

– research with traditional geometry that tries to find empirical equations for Nusselt number and optimal geometry for given working conditions [11, 12, 16, 17],
– modifications in wire geometry [18, 19] that includes the usage of serrated wire coils [19],
– combined implementation with other turbulators [4, 21], with modified inlet section [9], and
– with varying pitch and width [14, 22].

The future of this kind of turbulators belongs to varying wire shapes and dimensions, optimized geometry that changes along the length, and implementation in combination with nanofluids. Wires are used for manufacturing another type of turbulators: conical springs, which are also known as conical wire coils. Their influence on heat transfer enhancement is investigated in [23, 24]. Convergent, convergent-divergent, and divergent arrangements are examined for the Reynolds numbers in the range of 4627 to 34000. The addition of a conical spring top (CT) to a wire coil free-end is relatively simple for fabrication and does not hinder its surface cleaning task, see fig. 1(b).

Regarding the previous, the goals are: to find the optimal velocity of flue gas for temperatures in the range between 150-300 °C in pipes with wire coil turbulators, and to investigate the addition of CT to the free-end of wire coils on heat transfer enhancement.

In contrast to the previously quoted papers, in the examined case, together with convective, radiative heat transfer from the flue gas also exists. In the examined temperature range, the radiation is not negligible, particularly when Re < 10000. According to the authors' knowledge, there is no date on the design with CT in the open literature. Additionally, because of the varying gas amount and composition, it is difficult to experiment with turbulators when the medium is flue gas that originates from the combustion of solid biomass.

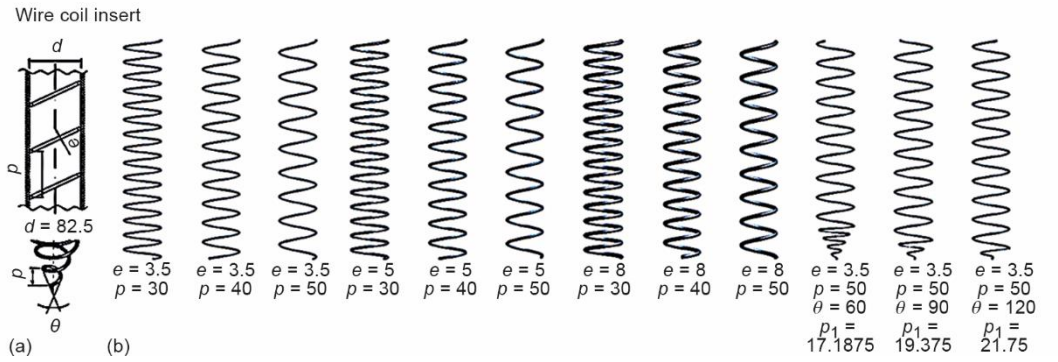

Figure 1. The examined wire coils and their basic geometry [mm]

Methodology

Figure 1(a) shows geometric parameters for a typical wire coil, whereas fig. 1(b) shows the examined designs. Wire coils are examined for the dimensionless pitch p/d in the range between 0.36-0.61, dimensionless wire diameter e/d = 0.04-0.1, and pitch to wire diameter ratios p/e = 3.75-14.3. Wire coils with CT are examined for the top angles of 60°, 90°, and 120°, wire diameter of 3.5 mm, and the pitch in the conical part between 17-22 mm. The examinations are carried out with a CFD model. To validate the model, in situ experimental investigations with a wood log gasification boiler were performed. To appraise radiative heat transfer and validate heat transfer in a smooth pipe, an existing cell model [25] is used. Several criteria are used to evaluate the performances of different wire coil designs in a given pipe.

Experimental investigations

A wood log gasification boiler, see fig. 2, with a nominal capacity of 18 kW was tested to examine the performance of wire coil turbulators and validate numerical models. After passing through gasification and combustion chambers, flue gas enters into a tubular heat exchanger that consists of three parallel pipes, each with an inner diameter of 82.5 mm. To prevent the buildup of solids and improve heat transfer, the pipes are equipped with wire coils with a diameter of 5 mm and a pitch of 40 mm. Each opening of a large hopper door activates a shake-off mechanism consisting of levers. The boiler operates with approximately constant heat output and oxygen concentration in the flue gas. However, during the startup and refueling or low levels of fuel in the hopper, neither the heat output nor the emissions are constant. The primary and secondary combustion air, as well as the fan speed, positions 5, 11, and 12 in fig. 2(b), are automatically controlled. The amounts of primary and secondary air are controlled to achieve the set exit temperature and oxygen level in the flue gas, respectively. During the experiments, the set exit flue gas temperature and the amount of oxygen were 150 °C and 7 vol.%, respectively. These are standard operating conditions for this commercially available boiler.

Figure 2 and tab. 1 show the experimental details. Dry and a few years old beech wood logs were used as a fuel source. Their ultimate and proximate analyses were taken from [26] as they originated from the same forest and were frequently used in the laboratory for testing. Before the testing, wood log moisture content was measured and was always in the range of 5.5-6.8 wt.%, Position 9 in tab. 1). After the boiler entered into a steady operation, the following quantities were simultaneously measured: flue gas volume flow rate, tempera-

ture, and composition, Positions 5-8 in fig 2(b) and tab. 1, water volume flow rate and its temperatures in characteristic points – 10, volume flow rates of primary – 11 and secondary – 12 combustion air, and flue gas temperatures at the entrance – 1, exit – 3, and at the distance 80 mm from the entrance – 2) of the pipe with wire coils. Figure 3 shows a 23-minute-long measurement session. In the figure, each point represents an average minute value, obtained as an average of six samples. The variations of the temperatures are in phase and decrease towards the boiler exit. This is a typical session, although there were sessions with smaller temperature variations, which depend on: the amount and properties of the fuel in the hopper, the effect of bridging in the gasification chamber, and the oscillations of water temperature. Because of the variations, the average temperatures are used for the validation of the CFD model.

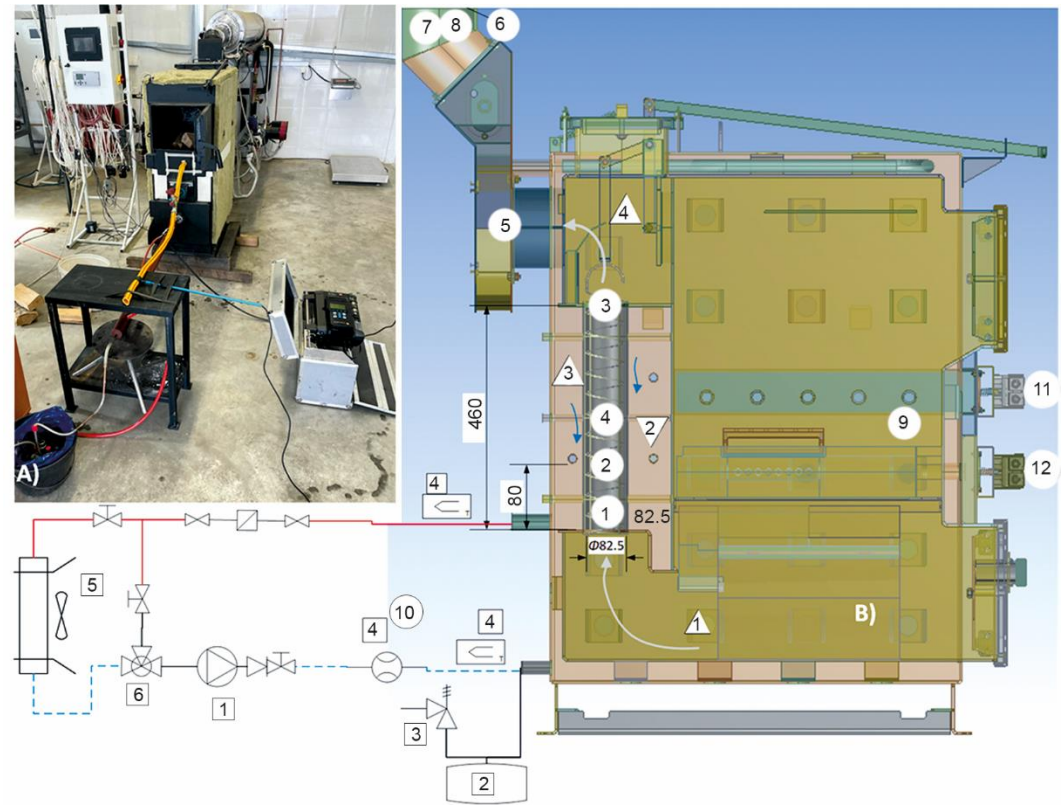

Figure 2. (a) Photo taken during the measurements and (b) experimental set-up; in triangles: *1 – combustion zone, 2 – water flow, 3 – wire coil, 4 – shake-off mechanism;* **in squares:** *1 – water pump, 2 – expansion tank, 3 – safety valve, 4 – heat meter, 5 – air cooling system, 6 – mixing valve*; **Encircled numbers symbolize measuring points, which are presented in tab. 1.**

The composition and flow rate of the flue gas were measured to calculate the heat transferred in the examined pipe. The composition was continuously monitored, whereas the oxygen level was additionally controlled by a λ probe, which is a part of the control system. Table 2 shows the average flue gas composition during the temperature measurements shown in fig. 3. Compared with temperature variations, the flue gas composition less fluctuates during the steady operation of the boiler.

Table 1. Measuring points (following Fig. 2), quantities, devices, and errors.

Measuring point	Quantity	Device	Error (absolute or relative)
1, 2, 3	Flue gas temperature	Testo 350 xl Type K TC	±0.4 °C (–100-200 °C) ±1 °C (200.1-1370 °C), resolution 0.1 °C
4	Volume flow rate	Testo 350 xl Combi S	0.1 m/s (0 to +40 m/s) ±16%
5	Temperature O_2 content	Boiler sensors	±1 °C ±0.1 vol%,
6	Volume flow rate	Testo 350 xl Combi S	m/s (0 to +40 m/s) ±7%
7	Flue gas composition	Testo 350 xl and Horiba ENDA 5000	O_2 ±0.8%, CO ±10 ppm, NO_x ±5%, SO_2 ±10 ppm (maximal errors in the measuring range)
8	Particulate emissions	Zambelli ZB1	±10%
9	Fuel composition and heating value, consumption, moisture content	Measuring report with the same fuel weight Testo 616	№ 10368 [26] – – ±0.1%
10	Delivered heat Water flow	Multical 303 – Kamstrup	±(0.15 + 2/Δ*t*)% calculator ±(1 + 0.01 V/V_N)% flow rate
11,12	Volume flow rate – primary combustion air	JDC Electronic SA vane anemometer Testo 410 a	±2% ±(0.2 m/s + 2 % of mv)
13	Pressure difference	Testo 521-1	±0.2%

The total flow of the flue gas was measured six hydraulic diameters away from the nearest flow disruption (elbows) in 10 measuring points. The measurement uncertainty was 7%. Compared with it, the measurement uncertainty of 16% for the volume flow rate through the examined pipe was noticeably larger. The flow is measured in the middle of the examined pipe in four measuring points. Nevertheless, the symmetrical flow pattern from the combustion chamber to the pipes and to a common outlet zone, see fig. 2(b), and slow velocities of the flue gas favor equal flow distribution through the three parallel pipes. This fact is additionally supported by: the measured flow fractions through the examined pipe that was in the range of 32.8-33.9% of the total flow, and the CFD simulation of the boiler. These facts additionally support the confidentiality of the flow measurements through the examined pipe. As the flow is measured, Position 4 in fig. 2(b) prior to and after the temperature measurements ①-③, during the latter measurements, the total ⑥

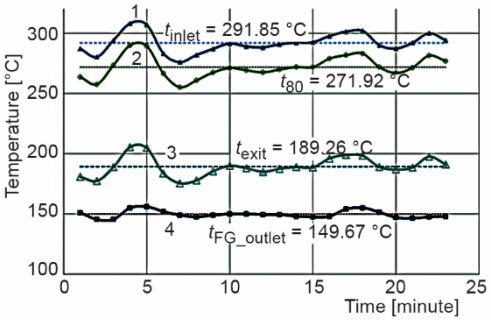

Figure 3. Temperature variations and their average values; *1 – at the pipe inlet, 2 – at the distance of 80 mm from the inlet, 3 – at the pipe outlet, and 4 – at the boiler outlet*

and flows of primary ⑪ and secondary air ⑫ were controlled. Taking into account all these facts, similar uncertainties for total and flow measurement through the examined pipe can be assumed.

Table 2. The average flue gas composition determined during the temperature measurements shown in fig. 2; dfg – in dry and wfg in the wet flue gas

Gas	Average value	Unit	Error (abs. or relative)
CO	143-dfg	ppm	±7ppm
NO_x	109-dfg	ppm	±5.5ppm
CO_2	12.474-wfg	%	±0.2%
H_2O	9.832-wfg	%	calculated (air+fuel)
N_2	71.322-wfg	%	calculated (air+fuel)
O_2	6.361-wfg	%	±0.8%
SO_2	0.004-wfg	%	±5ppm

The boiler design, see fig. 2(b) and measured water flow enable the calculation of water velocity around the examined pipe. The water temperature was raised less than 1 °C by heat exchange with the flue gas in the pipe. The reason was high water flow rates that varied from 1.41 to 2.23 m^3/h. For the most frequently used flow rate of 1.84 m^3/h, the total temperature rise in the boiler was 8.7 °C. The heat transfer rate from the flue gas was checked by the enthalpy rate of the water.

Considering low flue gas velocities, which were in the range of 0.95-1.2 m/s, and a short pipe length of 460 mm, the pressure difference between the inlet and outlet cross-sections (measuring points 1 and 3) was very small. Consequently, the literature data [12, 27] is used for validation of the pressure drop calculated by the CFD model.

The CFD model

A commercially available software ANSYS and its integration module FLUENT 18.1 was used to examine the wire coil designs. The software was validated by comparison with in-situ experimental investigations. In all simulations, the inlet/outlet pair: mass-flow-inlet/pressure outlet was used for the boundary condition. For all fluids, this is the most stable and the most frequently used pair of boundary conditions [28] defined by the mass-flow rate, the temperature of the fluid at the inlet, and the relative pressure of 0 Pa at the outlet. For the outer walls of the water domain, the adiabatic boundary condition was used. Figure 4(a) depicts the 2-D fine mesh grid of the model and the domains that were used for the numerical simulations, whereas tab. 3. shows the details of the mesh metrics. The mesh grid consists of 2657158 to 9888211 elements and 1469611 to 4130496 nodes. Nevertheless, the mesh quality is high because its maximum skewness is 0.224, and the minimum orthogonal quality is 0.779, both within the acceptable limits (0.94 maximum and 0.1 minimum, respectively) for a smooth numerical convergence [29]. The model uses the energy equation, the standard k-ε turbulent model, and the P1 radiation model. To solve the model, the SIMPLE scheme is used. The absolute convergence criterion was that the residual for energy and all other quantities were less than $1 \cdot 10^{-04}$ and 0.001, respectively. The set convergence criteria were met before 600 iterations. The total number of numerical simulations was 110.

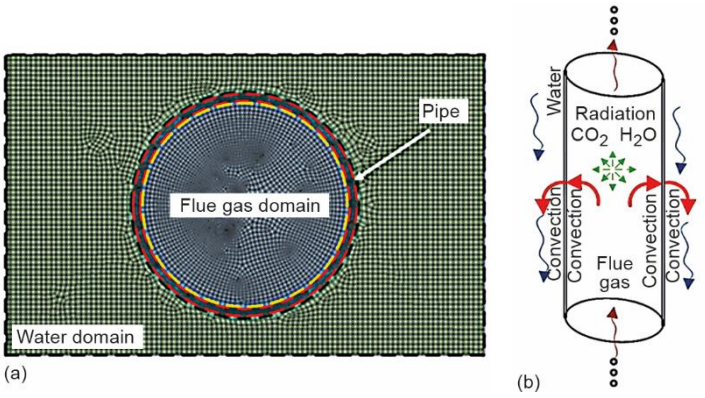

Figure 4. (a) The 2-D detail of the fine mesh grid with domains in the CFD model and (b) the principle of the cell model

Table 3. The details of the mesh

Examined design	Statistics		Element quality	Aspect ratio	Jacobian ratio	Skewness	Orthogonal quality
	Elements	Nodes					
DN80 – smooth pipe	3199973	3578776	0.958	1.212	0.935	0.065	0.989
DN80 – e = 3.5 mm, p = 40 mm*	7589669	1839126	0.844	1.813	0.997	0.222	0.781
DN80 – e = 5 mm, p = 40 mm*	6923421	1732361	0.844	1.812	0.997	0.222	0.781
DN80 – e = 8 mm, p = 40 mm*	6678958	1710928	0.845	1.813	0.997	0.222	0.782
DN80 – e = 3.5 mm, p = 40 mm, θ = 60°**	8426814	1976509	0.843	1.817	0.997	0.224	0.779
DN80 – e = 3.5 mm, p = 40 mm, θ = 90°**	8462312	1988508	0.843	1.817	0.997	0.223	0.779
DN80 – e = 3.5 mm, p = 40 mm, θ = 120°**	8953769	2078071	0.843	1.818	0.997	0.224	0.779

* wire coils and ** wire coil with CT

Cell modeling method

The model is composed of finite cells, which size is limited by the range of validity of the applied convective heat transfer models. Figure 4(b) shows the principle. Each cell of the model has three energy rate balance equations:

– heat flow rate from the flue gas is transferred by convection and gas radiation to the inner surface of the pipe eq. (1),
– this heat flow rate is then transferred by conduction to the outer surface of the pipe eq. (2), and
– where is by convection transferred to the water eq. (3):

$$\dot{Q} = \dot{m}_{\mathrm{fg}} c_{p_{\mathrm{fg}}} (t_{\mathrm{in}_{\mathrm{fg}}} - t_{\mathrm{out}_{\mathrm{fg}}}) = \dot{Q}_{\mathrm{con}} + \dot{Q}_{\mathrm{rad}_{i-i}} + \dot{Q}_{\mathrm{rad}_{i-(i-1)}} + \dot{Q}_{\mathrm{rad}_{i-(i+1)}} \quad (1)$$

$$\dot{Q} = \frac{t_{\text{wall,in}} - t_{\text{wall,out}}}{\frac{1}{2\pi\lambda_{\text{steel}}} \ln \frac{d_{\text{out}}}{d}} \tag{2}$$

$$\dot{Q} = \dot{Q}_{\text{con,w}} \tag{3}$$

where $\dot{Q}$ is the total heat flow rate and $\dot{Q}_{\text{con}}$ – the convective heat transfer rate from the flue gas to the pipe wall. To determine this quantity, the heat transfer coefficient is calculated by three equations presented in [27]. These are used depending on the character of flow: for laminar, the equation developed by Martin, for turbulent flow, the equation suggested by Gnielinski *et al.* [27], and for the transition region, an interpolation equation also suggested by Gnielinski.

The radiative heat transfer rate, $\dot{Q}_{\text{rad},i-i}$, between the flue gas and the pipe is calculated by the analytical method for calculation of the emissivities and absorptivities of H_2O, CO_2, and their mixtures presented in [30]. The last two terms on the right-hand side of eq. (1) that represent radiative heat transfer rates between adjacent cells are neglected. The convective heat transfer rate $\dot{Q}_{\text{con}}$ [W] from the pipe outer wall to the boiler water is determined by known geometry, and by calculating the heat transfer coefficient for the cylinder at rest in longitudinal flow presented in [31]. Basic temperature-dependent thermodynamic properties are taken from [32, 33]. The model is validated in [25] except for the convective heat transfer rate from the outer pipe wall to the water. This term has the smallest heat transfer resistance in the overall heat transfer coefficient, and, like all other submodels, comes from a reliable and confirmed source [31].

Validation of the CFD model

The results from the CFD simulations were compared with the in-situ measurements. Table 4 shows the comparison for two measurement sessions. In all comparisons, the boundary conditions for the CFD model were the inlet condition of the flue gas, which were taken from the measurements. For the first comparison in tab. 4, tab. 2 shows the flue gas composition, whereas fig. 3 shows measured temperatures. The shown comparisons show a good correlation. In other measurements, the maximum differences between the average measured flue gas exit temperature and heat flow rate with CFD predictions were 4.2 °C and 3.6%, respectively. The values for friction factor and Nusselt number are additionally compared to the experimental results from the literature in the results section.

Table 4. Comparison of measured and CFD data for the examined pipe (*d* = 82.5 mm, *e* = 5 mm, *p* = 40 mm)

	Measured value	Uncertainty	CFD prediction	Measured value	Uncertainty	CFD prediction
Boiler th. power [kW]	17.42	±0.39%	–	18.11	±0.38%	–
Mass flow rate [kgs^{-1}]	0.003766	±7%	BCS	0.003917	±7%	BCS
Inlet temperature [°C]	291.8	±1 °C	BCS	297.8	±1 °C	BCS
Outlet temperature [°C]	189.26	±0.4 °C	188.02	193.6	±0.4 °C	192.22
Heat flow rate [W]	424	±6.98%	429	449	±6.98%	454

* BCS – boundary condition for the CFD model

For a smooth pipe, the difference between friction factors, obtained for the CFD model and the Konakov equation, taken from [27], differ in the range between 2.1-8.3%. Figure 5 shows the comparison between the cell and CFD models for the smooth pipe with the dimensions as the examined one. There is a good correlation. The difference is at high Reynolds numbers that are not used in the examined design.

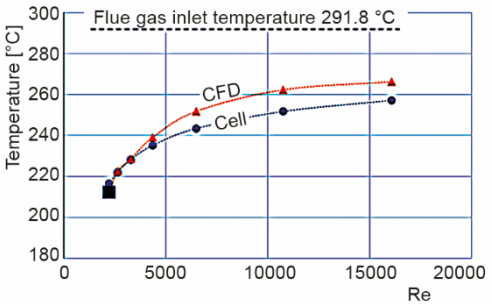

Figure 5. The comparison of the flue gas exit temperature predicted by the cell and CFD model for the smooth pipe with the same dimensions as the examined one

Performance evaluation

The most common criterion for the evaluation of thermohydraulic performances of the enhancement techniques is the overall enhancement ratio. It is defined as the ratio of the heat transfer enhancement ratio to the friction factor ratio [4]. When the ratio is used to compare different passive enhancement techniques at the same pumping power, it is also known as the performance evaluation criterion (PEC) [14]:

$$PEC = \frac{\mathrm{Nu}}{\mathrm{Nu_p}}\left(\frac{f}{f_\mathrm{p}}\right)^{-\frac{1}{3}} \tag{4}$$

where the pairs (Nu and f) and ($\mathrm{Nu_p}$ and f_p) denote the Nusselt number and friction factor for the pipe with wire coils and in the plain pipe, respectively. In eq. (4), the Fanning friction factor is determined by:

$$f = \frac{\rho\pi^2 d^5 \Delta p}{32 l \dot{m}^2} \tag{5}$$

where $\dot{m}$ is the mass-flow rate of the flue gas, ρ – the density at the average temperature, and Δp –its pressure drop in the pipe. Wire coils enhance convective heat transfer, and in the examined temperature range, they act as an additional finned surface for the thermal radiation of the gas mixture. To avoid the influence of the radiative heat transfer, the Nusselt number is calculated by:

$$\mathrm{Nu} = \frac{(\dot{Q} - \dot{Q}_\mathrm{rad})d}{\lambda A \Delta T_\mathrm{m}} \tag{6}$$

where $\dot{Q}$ is the total heat flow rate, $\dot{Q}_\mathrm{rad}$ – the radiative heat transfer rate, d = 0.0825 m – the pipe diameter, λ – the thermal conductivity of the flue gas, A = 0.119 m^2 – the surface area of the pipe, and T_m – the mean logarithmic temperature difference:

$$\Delta T_\mathrm{m} = \frac{t_{\mathrm{in_{fg}}} - t_{\mathrm{out_{fg}}}}{\ln\left(\dfrac{t_{\mathrm{in_{fg}}} - t_{\mathrm{wall,in}}}{t_{\mathrm{out_{fg}}} - t_{\mathrm{wall,in}}}\right)} \tag{7}$$

where $t_{\text{in,fg}}$ and $t_{\text{out,fg}}$ are the inlet and outlet temperatures of the flue gas, respectively, and $t_{\text{wall,in}}$ – the average inner temperature of the pipe surface.

In the examined case, there is a radiative heat transfer from the gas mixture to the pipe wall. Therefore eq. (4) is slightly changed to account for the total heat transfer and the limited pipe length. The Nusselt number is changed with total heat transfer, whereas in the denominator of eq. (6), the Fanning friction factor is changed with the total pressure drop, *i.e.*:

$$PEC_2 = \frac{Q}{Q_\text{p}}\left(\frac{\Delta p}{\Delta p_\text{p}}\right)^{-\frac{1}{3}} \tag{8}$$

where the pairs Q and Δp, and Q_p and Δp_p denote the total heat flow rate and friction factor for the pipe with wire coils and in the plain pipe, respectively.

As the flue gas pipes of a biomass gasification boiler should be equipped with turbulators, which would simultaneously enhance heat transfer and prevent fouling, the basis for comparison should be the existing design. To compare it with other wire coils, a coefficient of performance [15] is used:

$$COP = \frac{\Delta\dot{Q}}{\left(\frac{\dot{m}}{\rho}\right)\Delta p} \tag{9}$$

The COP indicates the magnitude of the heat transfer augmentation, $\Delta\dot{Q}$ *vs.* the enhancement of the pumping power, $\dot{m}\Delta p/\rho$, [15]. Additionally, it can be applied without the differences, $\Delta\dot{Q}, \Delta p$, to evaluate the performance of each wire coil in given conditions. In that case, instead of the difference in pressure drops between two designs, the total pressure drop of each design Δp should be used. This coefficient is marked with COP_2, and unlike COP in the denominator, there is the electrical power required to overcome the pressure drop in the pipe:

$$COP_2 = \frac{\dot{Q}}{\left(\frac{\dot{m}}{\rho}\Delta p\right)/\eta_\text{p}\eta_\text{el}} \tag{10}$$

This is an absolute indicator that represents the ratio between the heat transfer rate and the electric power used for pumping, assuming that it is produced by the same fuel as the transferred heat. The examined boiler and similar designs always have an electrical fan for forced circulation of the flue gas. As this is a small boiler, the efficiency of a small fan is assumed $\eta_\text{p} = 0.4$ [34]. The average electrical efficiency for the production of electricity from biomass is taken to be $\eta_\text{el} = 0.25$, [35].

Results and discussions

All analyses are carried out for the same pipe as the examined one ($d = 82.5$ mm, $l = 460$ mm) with the same inlet temperature of 291.8 °C of the flue gas, whose composition is given in tab. 2. A relatively short length simulates the performance of wire coils with and without a CT in small wood log boilers. To properly clean the surface of the examined pipe, the applicable wire coil pitches are in the range between 30 and 50 mm, whereas wire diame-

ters are between 3.5 and 8 mm. The simulations use discrete Reynolds numbers that are together with the corresponding mass flow rates of the flue gas shown in tab. 5.

Table 5. Reynolds numbers and corresponding mass flow rates

Reynolds number	2207	2637	3281	4353	6492	10759	16081
Mass-flow rate [kgs^{-1}]	0.00377	0.00452	0.00565	0.00753	0.0113	0.0188	0.0282

The higher the Reynolds number, the higher the total transferred heat. Figure 6. depicts this fact. For the same Reynolds number and pitch, the largest diameter has the highest total heat transfer rate. Larger wire diameters promote flow separation downstream of the wire and consequently enhance heat transfer. This is visible in fig. 7 Garcia *et al.* [13] stated, there are two effects that wire coils produce in the flow structure: rotation of the core flow and flow separation downstream of the wire. Both are visible in fig. 7. The rotation of the core flow is less pronounced because of the short length of the examined pipe. In the examined range, shorter pitches also enhance heat transfer, see fig. 6, and both effects that wire coils have on the flow structure, fig. 7. However, small dimensionless pitches decrease the Nusselt number and hence the total heat transfer, as was concluded by Hong *et al.* [14]. The short dimensionless pitches are not examined because they are unsuitable for the prevention of surface fouling.

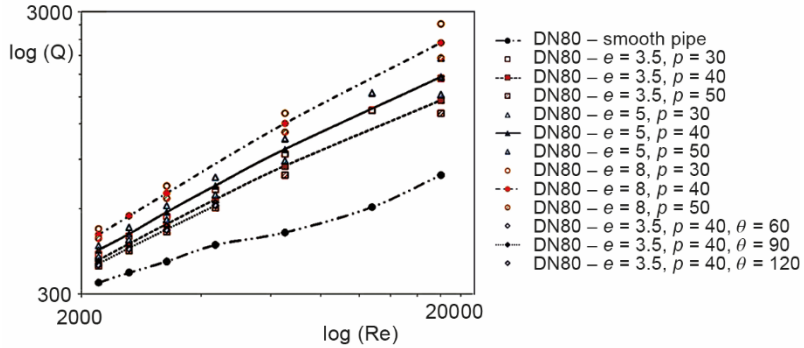

Figure 6. The total heat transferred in the examined pipe depending on the type of wire coils and the Reynolds number.

Wire coils also serve as a sort of radiation fins, but at the examined temperature range, the effect is negligible. Compared to the total heat transfer, the thermal radiation of the gas mixture is the largest at low Reynolds numbers and amounts from 13% at Re = 2207 to less than 2% at Re = 16081. The thermal radiation has the highest impact on total heat transfer in the smooth pipe at the lowest Reynolds number.

Figure 8 shows the friction factor, obtained by eq. (5), depending on the Reynolds number and wire coil type. Although the pipe is short, the data for the smooth pipe show a good correlation with the well-known Blasius equation. The largest discrepancy is at the beginning of the transition flow. The data obtained for wire coils show a positive correlation with the empirical equation suggested by Garcia *et al.* [12]. The maximal deviation is 13.3%. Garcia *et al.* obtained the empirical equation after a large number of experiments with water and water-propylene glycol mixtures.

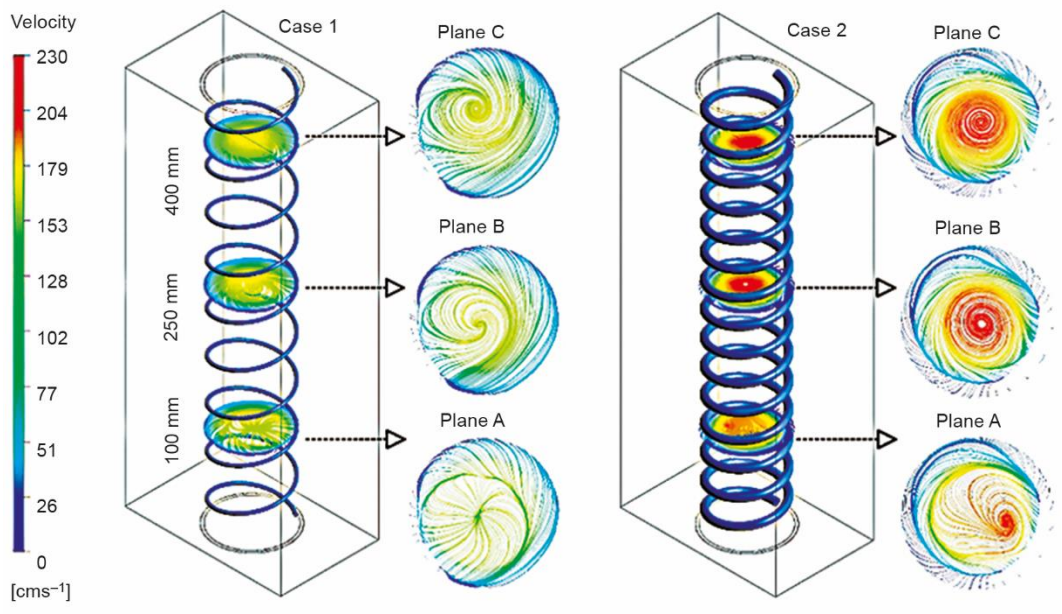

Figure 7. The velocity field inside the examined pipe with wire coils; Case 1 – wire coil with *e* = 3 mm, *p* = 50 mm, Case 2 – *e* = 8 mm, *p* = 30 mm

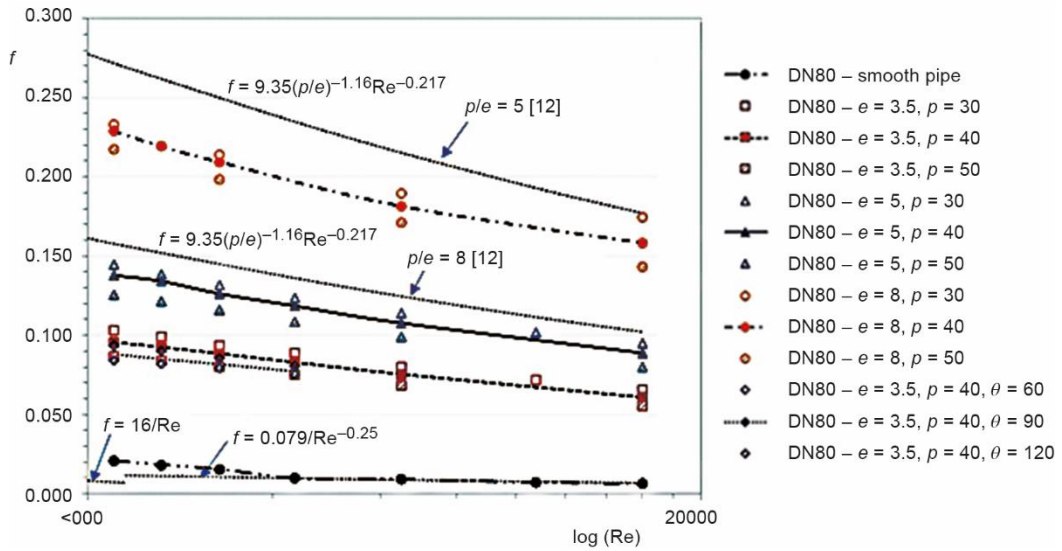

Figure 8. Friction factor depending on the wire coil type

To evaluate the examined designs, the Nusselt number is calculated based on eq. (6) and depicted in fig. 9. Although the pipe is short, the obtained values agree with the predictions of Garcia *et al.* [12]. Their empirical eq. (12) is shown in fig. 9 and does not account for the wire diameter. The figure shows that the largest dependency of the Nusselt number on the pitch is for the largest wire diameter.

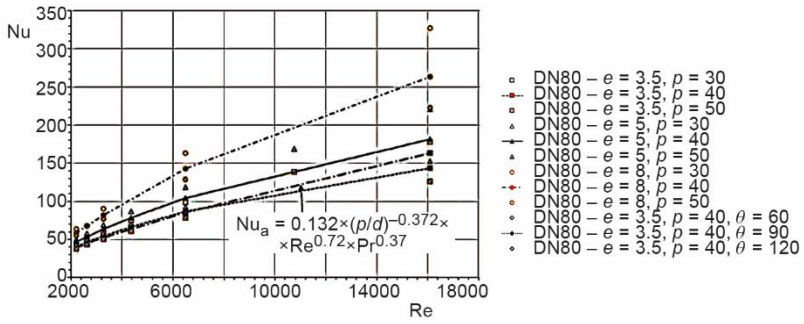

Figure 9. Nusselt number depending on the Reynolds number and the type of wire coils

To prevent fouling, the examined pipe needs a wire coil. Because of that, the COP eq. (9) compares the examined designs with the existing one (e = 5 mm, p = 40 mm) for six different Reynolds numbers. Figure 10 shows the comparison. The largest improvement is at low Reynolds numbers, and interestingly for the same wire diameter of 5 mm. Compared with the negative effect on the pressure drop, the decrease of the pitch by 10 mm has a higher positive effect on the heat transfer. In this case, a smaller pitch increases the COP. Regarding the findings of Hong *et al.* [14], the decrease of the pitch cannot be arbitrary as a very small pitch decreases the Nusselt number. The COP allows comparison among the designs and gives the optimal wire diameter by considering the heat transfer rate and pumping power.

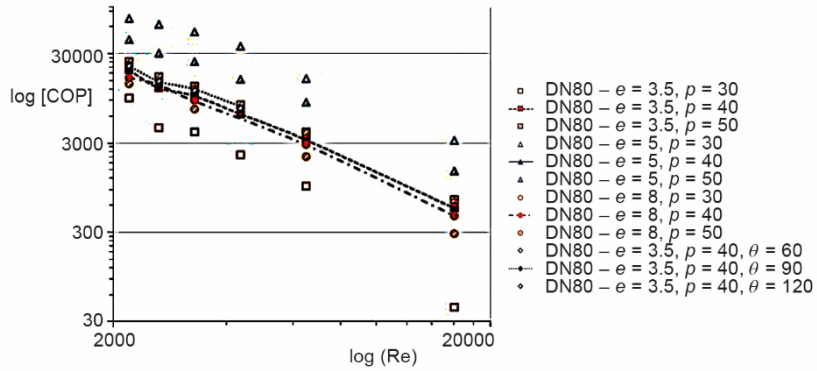

Figure 10. The relative COP based on the examined wire coil (e = 5 mm, p = 40 mm) depending on the Reynolds number for different designs

Figure 11. shows COP_2 depending on the Reynolds number and wire coil design. This is an absolute indicator calculated by eq. (10). The figure shows that the largest efficiency is at low Reynolds numbers. The smooth pipe has the largest efficiency because of a low-pressure drop in the laminar flow and low velocity that promotes a little higher radiative heat transfer. Among the designs with wire coils, the coil with the smallest diameter of 3.5 mm and the largest pitch of 50 mm has the highest efficiency. The previous data can be explained by the following facts:

– turbulators increase the pressure drop (*i.e.*, irreversibilities), and the toll for their usage is paid by a larger pressure drop,
– low efficiency (25%) for electricity production from biomass, and
– relatively low efficiency (40%) for converting electricity into the gas flow.

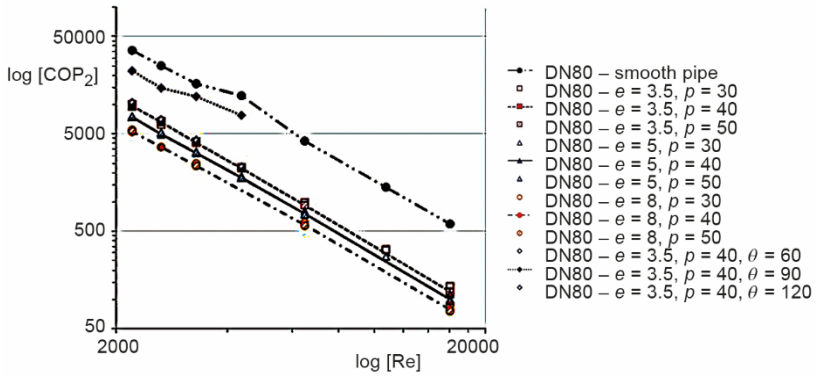

Figure 11. The absolute COP_2 depending on the Reynolds number for different designs

It is worth mentioning that among the designs with a wire diameter of 3.5 mm, the wire coil with the CT has the largest COP, see fig. 10. Additionally, fig. 11 shows that the design with CT has the highest COP_2 among wire coils. Figure 12 explains these facts. Namely, the CT causes the rotation of the core flow and compared with other wire coil types, it causes a smaller pressure drop in the inlet area.

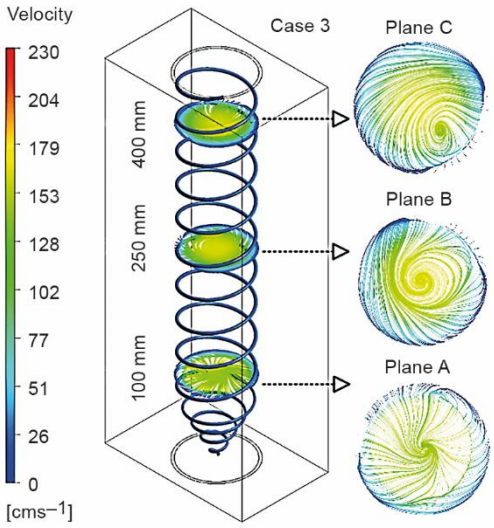

Figure 12. The velocity field inside the examined pipe equipped with the wire coil with CT (e = 3.5 mm, p = 40 mm, θ = 60º)

Turbulators have the highest impact on heat transfer enhancement in the transition region [13]. For this reason, fig. 13 shows PEC calculated by eq. (4). This is a general criterion used for the comparison of different types of turbulators. The PEC and PEC_2 have identical dependencies on the Reynolds number. Compared with PEC, PEC_2 is lower than 1. The PEC shows that the optimal range for the implementation of wire coils in the examined heat exchanger is for the Reynolds numbers between 2500 and 3500, *i.e.*, for the flue gas velocities at the inlet of the pipe in the range between 1.35 and 1.8 m/s.

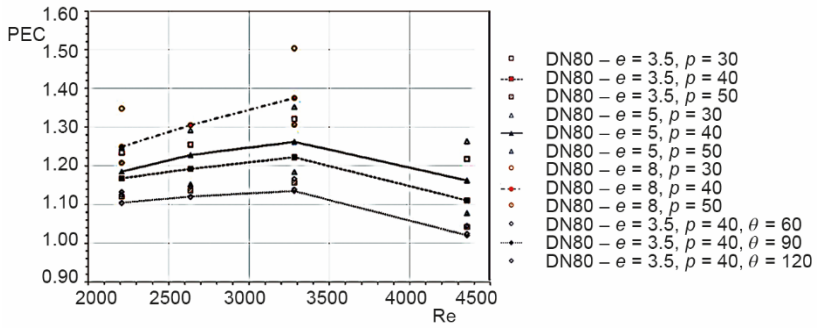

Figure 13. The PEC for low Reynolds numbers depending on the wire coil designs

Conclusions

Regarding the defined goals, presented results, and conducted measurements the main conclusions are as follows.

- In situ experimental investigations of wire coils or other turbulators in wood log gasification boilers are difficult because of the variation in the gas composition, temperatures, and flow rates. The reason is the batch combustion of wood logs.
- Compared with other parts of these boilers, the pressure drop in pipes with wire coils is often negligible. In that case, to obtain the highest heat transfer rate, the largest wire diameter with the smallest pitch that allows proper prevention of surface fouling should be used. The decrease in pitch cannot be arbitrary as very small pitches reduce the Nusselt number.
- The COP allows comparison among the designs that are simultaneously used to prevent fouling and enhance heat transfer and, for the same wire diameter and flow rate, gives the optimal one. A general criterium, like PEC, gives the optimal flow rates.
- The shorter the pipe with wire coils, the less pronounced the effect of the rotation of the core flow on the heat transfer enhancement. The addition of CT at the free end of wire coils can increase this effect and the efficiency of heat exchange.
- In the temperature range between 150-300 °C, the thermal radiation of the gas mixture has the largest impact on the turbulator efficiency at low Reynolds numbers.
- In the examined case, the optimal range for the implementation of wire coils is for the Reynolds numbers between 2500 and 3500, *i.e.*, for flue gas velocities at the inlet of the pipe in the range between 1.35 and 1.8 m/s. In the recommended range, higher velocities should be applied for longer pipes because of the gas cooling.

Acknowledgment

This research was supported by the Ministry of Education, Science and Technological Development of the Republic of Serbia (Grant Nos. 451-03-68/2022-14/200108 and 451–03-68/2022–14/200105 Integrated research in the field of macro, micro, and nanomechanical engineering).

Nomenclature

A	– surface area of the pipe, [m^2]	l	– length of the pipe
c_p	– specific heat capacity at constant pressure, [kJkg^{-1}K^{-1}]	$\dot{m}$	– mass-flow rate, [kgs^{-1}]

$\dot{m}\Delta p/\rho$ – enhancement of the pumping power, [W]
t – temperature, [°C]
$\dot{Q}$ – total heat flow rate, [W]
$\dot{Q}_{con}$ – convective heat transfer rate from the flue gas to the pipe wall, [W]
$\dot{Q}_{con,w}$ – convective heat transfer rate from the pipe outer wall to the boiler, [W]
$\dot{Q}_{rad_{i-i}}$ – radiative heat transfer rate, [W]
ΔQ – heat transfer augmentation, [W]
Q and Δp – Nusselt number and friction factor for the pipe with wire coils, [–]
d – diameters, [m]
f – friction factor, [–]
Δp – pressure drop, [Pa]
Q_p and Δp_p – Nusselt number and friction factor for the plain pipe, [–]
Nu – Nusselt number, [–]
T_m – mean logarithmic temperature difference, [K]
$t_{in,fg}$ – inlet temperature of the flue gas, [K]
$t_{out,fg}$ – outlet temperature of the flue gas, [K]
$t_{wall,in}$ – average inner temperature of the pipe surface, [K]

Greek symbols

λ – thermal conductivity, [$Wm^{-1}K^{-1}$]
η_P – efficiency of a small fan, [–]
η_{el} – average electrical efficiency, [–]
ρ – density, [kgm^{-3}]

Acronyms

CT – conical top
PEC – performance evaluation criterion

References

[1] Hassan, R., *Ecosystems and Human Well-Being: Current State and Trends*, Island Press, Washington DC, Vol. 1, 2005
[2] Cornette, J. F. P., *et al.*, Particulate Matter Emission Reduction in Small- and Medium-Scale Biomass Boilers Equipped with Flue Gas Condensers: Field measurements, *Biomass and Bioenergy, 148* (2021), Feb., pp. 1-9
[3] Hebenstreit, B., *et al.*, Techno-Economic Study of a Heat Pump Enhanced Flue Gas Heat Recovery for Biomass Boilers, *Biomass and Bioenergy, 71* (2014), Dec., pp. 12-22
[4] Liu, S., Sakr, M., A Comprehensive Review on Passive Heat Transfer Enhancements in Pipe Exchangers, *Renew. Sustain. Energy Rev., 19* (2013), Mar., pp. 64-81
[5] Moya-Rico, J. D., *et al.*, Experimental Characterization of a Double Tube Heat Exchanger with Inserted Twisted Tape Elements, *Appl. Therm. Eng., 174* (2020), Apr., ID 115234
[6] Karagoz, S., *et al.*, Experimental Investigation of the Effect of Wave Turbulators on Heat Transfer in Pipes, *Thermal Science, 26* (2022), 2C, pp. 1771-1783
[7] Alam, T., *et al.*, Heat and Flow Characteristics of Air Heater Ducts Provided with Turbulators – A Review, *Renew. Sustain. Energy Rev., 31* (2014), Mar., pp. 289-304
[8] Sarac, B. A., Bali, T., An Experimental Study on Heat Transfer and Pressure Drop Characteristics of Decaying Swirl Flow through a Circular Pipe with a Vortex Generator, *Exp. Therm. Fluid Sci., 32* (2007), 1, pp. 158-165
[9] Promvonge, P., Eiamsa-ard, S., Heat Transfer and Turbulent Flow Friction in a Circular Tube Fitted with Conical-Nozzle Turbulators, *Int. Commun. Heat Mass Transf., 34* (2007), 1, pp. 72-82
[10] Yakut, K., *et al.*, Performance and Flow-Induced Vibration Characteristics for Conical-Ring Turbulators, *Appl. Energy, 79* (2004), 1, pp. 65-76
[11] Kongkaitpaiboon, V., *et al.*, Experimental Investigation of Convective Heat Transfer and Pressure Loss in a Round Tube Fitted with Circular-Ring Turbulators," *Int. Commun. Heat Mass Transf., 37* (2010), 5, pp. 568-574
[12] García, A., *et al.*, Experimental Study of Heat Transfer Enhancement with Wire Coil Inserts in Laminar-Transition-Turbulent Regimes at Different Prandtl Numbers, *Int. J. Heat Mass Transf., 48* (2005), 21-22, pp. 4640-4651
[13] García, A., *et al.*, The Influence of Artificial Roughness Shape on Heat Transfer Enhancement: Corrugated Tubes, Dimpled Tubes and Wire Coils, *Appl. Therm. Eng., 35* (2012), 1, pp. 196-201
[14] Hong, Y., *et al.*, Heat Transfer and Fluid Flow Behaviors in a Tube with Modified Wire Coils, *Int. J. Heat Mass Transf., 124* (2018), Sept., pp. 1347-1360
[15] Gholamalizadeh, E., *et al.*, Study of Intensification of the Heat Transfer in Helically Coiled Tube Heat Exchangers via Coiled Wire Inserts, *Int. J. Therm. Sci., 141* (2019), Mar., pp. 72-83

[16] San, J. Y., *et al.*, Experimental Investigation on Heat Transfer and Fluid Friction Correlations for Circular Tubes with Coiled-Wire Inserts, *Int. Commun. Heat Mass Transf., 65* (2015), July, pp. 8-14
[17] Gunes, S., *et al.*, The Experimental Investigation of Heat Transfer and Pressure Drop in a Tube with Coiled Wire Inserts Placed Separately from the Tube Wall, *Appl. Therm. Eng., 30* (2010), 13, pp. 1719-1725
[18] Gunes, S., *et al.*, Heat Transfer Enhancement in a Tube with Equilateral Triangle Cross Sectioned Coiled Wire Inserts, *Exp. Therm. Fluid Sci., 34* (2010), 6, pp. 684-691
[19] Promvonge, P., Thermal Performance in Circular Tube Fitted with Coiled Square Wires, *Energy Convers. Manag., 49* (2008), 5, pp. 980-987
[20] Chompookham, T., *et al.*, Influence of a Novel Serrated Wire Coil Insert on Thermal Characteristics and Air Flow Behavior in a Tubular Heat Exchanger, *Int. J. Therm. Sci., 171* (2021), Jan., ID 107184
[21] Abbaspour, M., *et al.*, Heat Transfer Improvement in a Tube by Inserting Perforated Conical Ring and Wire Coil as Turbulators, *Heat Transf., 50* (2021), 6, pp. 6164-6188
[22] Singh, S. K., Sarkar, J., Improving Hydrothermal Performance of Hybrid Nanofluid in Double Tube Heat Exchanger Using Tapered Wire Coil Turbulator, *Adv. Powder Technol., 31* (2020), 5, pp. 2092-2100
[23] Karakaya, H., Durmus, A., Heat Transfer and Exergy Loss in Conical Spring Turbulators, *Int. J. Heat Mass Transf., 60* (2013), 1, pp. 756-762
[24] Keklikcioglu, O., Ozceyhan, V., Heat Transfer Augmentation in a Tube with Conical Wire Coils Using a Mixture of Ethylene Glycol/Water as a Fluid, *Int. J. Therm. Sci., 171* (2022), July, ID 107204
[25] Knežević, S. D., *et al.*, Radiant Recuperator Modeling and Design, *Thermal Science, 21* (2017), 2, pp. 1119-1134
[26] ***, ITEM Consult"ltd, "Test Report," Sofia, Bulgaria, 2018
[27] Gnielinski, V., G1 Heat Transfer in Pipe Flow, in: *VDI Heat Atlas*, Springer, New York, USA, 2010, pp. 691-700
[28] Dimitrios, S., Boundary Conditions & Solver Settings, 2013. https://events.prace-ri.eu/event/156/contributions/6/attachments/65/89/Fluent-Intro_14.5_L02_BoundaryConditionsSolverSettings.pdf.
[29] Athanasios, N., *et al.*, Optimization of a Log Wood Boiler Through CFD Simulation Methods, *Fuel Process. Technol., 137* (2015), Sept., pp. 75-92
[30] Vormeyer, Dieter, K. S., View Factors, in: *VDI Heat Atlas*, Springer, New York, USA, 2010, pp. 961-978
[31] Martin, H., *et al.*, Heat Transfer to Single Cylinders, Wires, and Fibers in Longitudinal Flow, in: *VDI Heat Atlas*, Heidelberg, Germany, 2010, pp. 717-721
[32] Kleiber, M., Joh, R., Properties of Selected Importanat Pure Substances, in: *VDI Heat Atlas*, 2nd ed., Springer, New York, USA, Germany, 2010, pp. 153-299
[33] Pfennig, A., *et al.*, Properties of Multicomponent Fluid Mixture, in: *VDI Heat Atlas*, Springer, New York, USA, 2nd ed, 2010, pp. 531-550
[34] ***, Engineering ToolBox, Fans – Efficiency and Power Consumption, 2003. https://www.engineeringtoolbox.com/fans-efficiency-power-consumption-d_197.html
[35] Kramreiter, R., *et al.*, Experimental Investigation of a 125 kW Twin-Fire Fixed Bed Gasification Pilot Plant and Comparison to the Results of a 2 MW Combined Heat and Power Plant (CHP), *Fuel Process. Technol., 89* (2008), 1, pp. 90-102

Paper submitted: July 5, 2022
Paper revised: December 17, 2022
Paper accepted: December 30, 2022